Research Department

Technical Report No. 73

Raw HIRS/2 radiances and model simulations in the presence of clouds

Rolando Rizzi

September, 1994

1. INTRODUCTION

Clouds exert a strong influence on the distribution of heating and cooling at the Earth's surface and within the atmosphere. This has long been recognized in climate studies and in the development of General Circulation Models (GCM) (*Slingo and Slingo*, 1989; *Browning*, 1994), much less in Numerical Weather Prediction (NWP), until the extension of useful forecast length and the diversification in the products range has given new impulse to the development of more accurate parametrizations of diabatic processes (*Ritter*, 1992).

When the new ECMWF prognostic cloud scheme (*Tiedtke*, 1993) becomes operational, the ECMWF model will acquire some capability to assimilate cloud-related information. To prepare further development, calibrated and earth located, or raw, TOVS (Tiros-N Operational Vertical Sounder) radiances are used as a diagnostic tool to evaluate the ability of sequences of short range forecasts, from different models, to simulate some of the features in the measured data. The present exercise is therefore quite different from the diagnostics which employ long term integrations of a model to test its average properties against some independent data set.

The main difference between the raw TOVS radiances used in the present exercise and the radiances used operationally at ECMWF (*Eyre et al*, 1993) is the cloud clearing process, whose aim is to identify and eliminate the data affected by clouds. Other differences will be discussed in section 2. Since the signature of clouds on upwelling atmospheric radiance is quite marked at visible and infrared wavelengths, inadequacies in model representations of the three dimensional structure of cloud cover and cloud liquid water are easily identified. One can therefore make a detailed examination of aspects of the hydrological cycle and energetics in current NWP models and in GCMs.

Although the importance of clouds in NWP lies mainly in their radiative effects, it is common practice to compare model cloud properties, such as cloud amount (either total or for thick layers) with "equivalent" quantities retrieved from data sets which are independent of the model, and are frequently derived from satellite radiance data (*Rossow and Schiffer*, 1985; *Hamill et al*, 1992; *Stowe et al*, 1991). In such a comparison the same name (for example total cloud amount) may be given to quite distinct quantities, obtained using different underlying assumptions (*Morcrette*, 1991a). Great care is needed when comparing these satellite products among themselves and with model products (*Hou et al* 1993). On the other hand when simulated radiances, obtained using all pertinent model information, are compared to measurements, one needs to be aware of the assumptions used in the simulations themselves. The evaluation of the errors is a delicate procedure in both cases, but the error estimation is particularly difficult for retrieved products such as total cloud cover.

This report presents the results of a comparison between a selected set of raw HIRS/2 radiances and simulations using the required model output fields. Estimates of outgoing longwave flux at the top of the atmosphere (OLR) are also obtained from a subset of HIRS/2 radiances. These are compared to OLR computed from the simulated radiances and to the OLR computed by the flux radiation scheme of the forecast model.

The present report is structured as follows:

Section 2: Preprocessing of TOVS data

Section 3: Forecast experiments

Section 4: adiance simulation in presence of clouds

Section 5: Results of radiance comparison

Section 6: Results of comparison of longwave fluxes at TOA

Section 7: Conclusions

Section 8: References

2. PREPROCESSING OF TOVS DATA

The data used in this work are measured by two sensors on board the NOAA polar orbiters: the HIRS/2 (High Resolution Infrared Radiation Sounder/2) and MSU (Microwave Sounding Unit). A description of the nominal characteristics of the instruments can be found in *Smith et al* (1979).

Two data sets have been processed:

- level 1-B HIRS/2 data from 12UT 8 February to 06UT 11 February, 1989;
- TIP (Tiros Information Processor) data from 00UT 14 October to 06UT 16 October 1993.

In October 1989 the operational satellites were NOAA-10 and NOAA-11, while in October 1993 they were NOAA-11 and NOAA-12. The statistical results for the two datasets need to be evaluated separately, because of the difference in platforms and in the forecast models that have been used for the radiance simulations. The equatorial crossing time (ECT) for the ascending (A) and descending (D) orbit portion for the three platforms is significantly different. Each instrument therefore senses the atmosphere and the surface at different local time of the day. The ECT itself varies slowly during each platform's lifetime because the spacecraft does not make an integral number of revolutions per day, and also because the orbit decays, due to atmospheric drag, and the satellite has to speed up, enhancing the variation. As a result the ECT (local time) for each platform and data set is approximately:

- NOAA-10: February 89: 19:35 (A) and 7:35 (D);
- NOAA-11: February 89: 13:45 (A) and 1:45 (D);
  October 93 : 16:10 (A) and 4:10 (D);
- NOAA-12: October 93 : 19:30 (A) and 7:30 (D).

Note the difference between NOAA-11 ECT in 1989 and 1993.

The ITPP (International TOVS Processing Package) (*Smith et al*, 1993) has been used to process the data and to produce calibrated and earth located radiances. During preprocessing two brightness temperature datasets were generated, with and without a number of 'corrections' which are usually applied during the operational satellite data processing performed by NOAA-NESDIS (National Oceanic and Atmospheric Administration - National Environmental Satellite, Data and Information Service). These corrections are limb correction of HIRS/2 and MSU data, correction of HIRS/2 window channels for water vapour attenuation, and correction for surface reflectivity and liquid water attenuation for MSU channels.

The spacing between HIRS/2 scanning lines is about 42 km and the spacing between Field of Views (FOVs) ranges from about 26 km at the centre of the scan to about 81 for the outer FOVs. The resolution of a field of HIRS/2 measurements can be defined as their mean spacing and is therefore about 40 Km. There is also a spatial averaging involved since FOV equivalent circular diameter ranges from about 17.4 km (FOV area of 235 km^2) to about 40km (1260 km^2). The resolution of HIRS/2 measurements is therefore higher than the model resolution which can be estimated to be between 80 and 90 km. To reduce the effect of sub-grid scale processes present in the measurements, each radiance field, and the OLR field, have been filtered, using a bi-dimensional gaussian filtering function (*Amato et al*, 1991), to reduce the resolution to about 90 km. In the following text any reference to measured radiances relates to filtered radiances unless otherwise stated.

A product of the processing is the OLR, computed from a regression which uses the corrected brightness temperatures of HIRS/2 channels 2 to 8 and 10 to 12 as predictors. This OLR estimate is referred to as OLRTOV in the rest of the paper. The regression is part of the ITPP but is practically undocumented. It is however analogous to the technique described in *Smith and Woolf* (1983) used to obtain longwave radiation flux from VAS channels (VISSR Atmospheric Sounder), where it is found that the regression explains 99.9% of the simulated OLR variance in the clear case with a standard error of 1.2 Wm^{-2}, and 99.8% with a standard error of 2.2 Wm^{-2} in the cloudy case. Because of the close similarity between VAS and HIRS/2 spectral channels used in the regression, it is likely that the error estimates found in the referenced paper are applicable to the regression part of ITPP for clear and cloudy situations separately. In the ITPP however only one set of coefficients is used for any atmospheric condition, clear or cloudy.

Ellingson et al (1989) have developed a similar technique to estimate OLR from HIRS/2 observations. Their regression analysis shows that 4 HIRS/2 channels are sufficient to explain 99.8% of the variance of the complete set of 3200 conditions with a root mean square error of about 2 Wm^{-2}. A validation of the technique is presented in *Ellingson et al* (1990) by comparing nighttime homogeneous NOAA-9 ERBE scanner derived OLRs to estimates based on collocated HIRS measurements. They find that their regression technique yields flux data which tend to be lower by about 1-3 Wm^{-2} with rms differences of the order of

4 Wm^{-2} in all except overcast conditions. In the latter case the HIRS estimates show a positive bias of 4 to 7 Wm^{-2} with rms differences in the range 6 to 10 Wm^{-2}. The authors conclude that the HIRS estimates agree with ERBE scanner observations about as well as different ERBE scanners agree with each other.

In view of these results one can expect the ITPP regression to provide an estimate with an rms error of less than 10 Wm^{-2}, including in the error budget the errors introduced by the brightness temperature corrections discussed above. Not much is known on systematic errors introduced by the ITPP regression. Since the same technique is applied to simulated and measured radiances (to produce respectively OLRSIM and OLRTOV), relative biases can be produced when the regression is applied to very different atmospheric situations, such as radiance measurements in a cloudfree area while simulated radiances contain a significant amount of clouds. In these conditions however the bias is much smaller than the difference in the two estimates.

Caution must however be used when comparing OLRTOV to the OLR computed by the forecast model (OLRMOD), since no bias correction is applied to the simulated radiances. The need for such a correction and the method employed operationally at ECMWF when assimilating cloud-cleared brigthness temperatures are described in *Eyre* (1992). The magnitude of the bias observed between cloud-cleared brightness temperatures over sea and simulations, based on collocated radiosonde measurements, is shown in Table 2.1, for February 1989 and October 1993 and for the channels used in the OLR regression. These monthly biases, and the associated standard deviations, will be referred to as 'clear' biases and 'clear' standard deviations. The expected bias in the computation of clear-sky OLR using the regression is also shown. A large positive bias is expected for NOAA-11 OLR estimates in 1993, which is mostly due to the considerable weight attributed to channel 10 and to the clear bias found for that channel in NOAA-11. In view of this, only results of OLR comparisons for the 1989 dataset will be discussed in section 6.

	FEBRUARY 1989		OCTOBER 1993	
ch	NOAA-11	NOAA-10	NOAA-11	NOAA-12
2	1.88	1.12	1.92	1.18
3	2.01	1.11	2.23	1.41
4	0.09	-0.12	-0.12	0.30
5	-0.15	-0.14	-0.19	0.10
6	0.09	0.01	0.06	0.04
7	0.19	0.07	0.15	0.23
8	0.23	-0.42	-1.55	-1.31
10	0.46	0.26	0.82	0.81
11	-0.12	0.11	0.89	0.94
12	-0.19	-0.33	0.95	0.51
OLR	3.42	-0.38	10.66	-3.79

Table 2.1 Mean monthly bias between simulated clear-sky and cloud-cleared brightness temperatures over sea, and mean expected OLR bias in clear-sky conditions.

3. FORECAST RUNS AND SPIN-UP EFFECT

Radiance simulations are based on model fields obtained from a short-range forecast so that the description of the dynamical fields is still accurate. In order to choose a suitable forecast length, in view of the operational model spin-up time, a comparison was made among OLR computed by operational forecasts of various lengths for midnight of every day in the period from October 1, 1992 to the end of February 1993.

It is found that the OLR field decreases slightly with increasing forecast length, an effect probably caused by an increase in mean cloudiness as convection becomes stronger. However the differences between OLRs from different forecasts tend to grow rapidly in root mean square sense, an effect probably caused by growing discrepancies in the circulation patterns generated by the forecasts. In view of these results, satellite data have been compared with simulations produced using the second day of the forecast for each day of data. It has been assumed that the spin-up time of the various versions of the forecast model used in the present paper is not longer than that of the operational model.

A number of forecast experiments were run, all at resolution T213 and with 31 vertical levels, involving 4 different versions of the forecast model:

1989 data i. Prognostic Cloud Scheme (PCS) within the operational spectral model (SPM) cycle 46 (PCS46);

ii. SPM cycle 46 (SPM46) used as control experiment;

1993 data: i. PCS within the operational spectral model (SPM) cycle 48 (PCS48);

ii. SPM cycle 48 (SPM48) used as control experiment.

In all cases the forecasts are started from initialized analyses produced by the assimilation system which was operational at the time the satellite data were measured: the first guess is obtained using cycle 31 model library (T106L19) for 1989 data and cycle 48 (T213L31) for 1993 data.

A complete description of the differences between the various experiments is beyond the scope of the present paper. Model changes between cycle 46 and 48 of the SPM involve the boundary layer and the land surface parametrizations (*Betts et al*, 1993). The parametrization of air-sea interaction has also been modified (*Miller et al*, 1992). A brief account of the salient differences between the experiments is given below with the aim of increasing the understanding of the differences found between simulated and measured data.

Clouds in SPM (both cycle 46 and 48) are determined diagnostically (*Slingo*, 1987). The cloud cover of stratiform clouds is diagnosed from the large scale values of relative humidity, vertical velocity and the

temperature lapse rate across boundary layer inversions. Convective cloudiness is diagnosed from the precipitation rate produced by the model convection scheme. Cloud water content is prescribed as the equivalent of a supersaturation of 5% for stratiform clouds and a fixed mixing ratio of 0.1 g/kg for convective clouds.

The PCS applied to both cycles 46 and 48 is described in *Tiedtke* (1993). It is a prognostic approach where the time evolution of the cloud variables, cloud cover and cloud water content, is determined by the sources and sinks due to the various cloud processes, i.e. clouds form as the result of adiabatic and diabatic cooling, cumulus convection and boundary layer turbulence and clouds dissipate through adiabatic and diabatic heating, turbulent mixing of cloud air with unsaturated environmental air and precipitation processes. An important feature of this scheme is the explicit representation of anvil and cirrus clouds in connection with penetrative cumulus convection. Their time evolution is determined by the horizontal advection of condensate, from convective updrafts into environmental air and by precipitation processes, large scale lifting and radiative transfer. In the current version of PCS the horizontal advection term is not accounted for. The treatment of the precipitation process for ice, which plays a dominant role for the maintenance of the ice content, is based on *Heymsfield and Donner* (1990) in that the loss of cloud ice is determined by sedimentation of ice crystals where fallspeeds are used in agreement with observational data.

In Cycle 48 of SPM a skin layer has been introduced over land with no heat capacity so that its temperature adjusts instantaneously to the radiative forcing. Some decoupling is obtained between surface and lower atmosphere so that the surface temperature is allowed to increase during daytime without increase of 2-metre temperature and soil heat flux. In cycle 46 the upper surface layer is a 7.2 cm deep homogeneous layer and the surface temperature is the average soil temperature of the upper layer.

4. RADIANCE SIMULATION IN PRESENCE OF CLOUDS

Radiances for a clear atmosphere are computed using surface skin temperature and the temperature and humidity profiles. The simulation of cloud effects requires additional input fields, namely Cloud Fraction (CF) and Cloud Liquid Water (CLW).

The current operational procedure consists of postprocessing any 3-d variable as a truncated set of spectral coefficients. Truncation effects are particularly evident for fields, such as CF and CLW, which may show large variations from one grid point to the next. Negative values are found in the retrieved CF and CLW fields, which can be filtered out; values of CF larger than unity can be filtered out as well while overshoots in the CLW fields are generally not simple to identify.

Table 4.1 lists, for each model level (first column), the number (and percentage) of negative CLW and CF values (column 2 to 5), the number of points in which either CF or CLW are negative (1.OR.2) and, in the last two columns, the number of points (and percentage) in which CF is greater than unity. The forecast is an SPM46 T213L31 for 00UT of 9 February 1989, retrieved at T106 resolution on a regular grid. The overall effect on cloudiness is shown in the scatter plot of figure 4.1. TCC MODEL (abscissa) is MARS parameter 164, a 2-d grid point field without any spectral conversion; the ordinate is Total Cloud Cover, computed using the same algorithm used to compute parameter 164, but starting from the retrieved CF (and CLW) fields (TCCMP). At grid points in which the model level value of either CF or CLW is negative, a value of zero is assumed; similarly a model level value of CF larger than unity is reset to the latter value. The mean difference among TCC MODEL and TCC is 0.08 while the root mean square difference is 0.12. The bias is positive indicating that the effect of spurious clouds being generated in the model spatial domain overcomes the filtering out of real cloud features, caused by the negative values found at grid points close to a CF (or CLW) discontinuity. These spurious clouds tend to maximize their effect since the small positive values, found away from the bulk of cloud features, possess a small interlevel correlation and are thus randomly summed.

(1) LEVEL	(2) CLW<0	%	CF<0	%	1.OR.2	%	CF>1	%
1	0	0.00	0	0.00	0	0.00	0	0.00
2	0	0.00	0	0.00	0	0.00	0	0.00
3	0	0.00	0	0.00	0	0.00	0	0.00
4	25455	49.72	25424	49.66	32827	64.12	40	0.08
5	24942	48.71	24555	47.96	37057	72.38	444	0.87
6	25211	49.24	24735	48.31	36912	72.09	142	0.28
7	24844	48.52	24311	47.48	35954	70.22	253	0.46
8	24471	47.79	24062	47.00	35114	68.58	286	0.58
9	24332	47.52	23667	46.22	34838	68.04	342	0.67
10	23702	46.29	23265	45.44	34306	67.00	445	0.87
11	23408	45.72	22661	44.26	33313	65.06	577	1.13
12	23011	44.94	21866	42.71	32995	64.44	647	1.26
13	22108	43.18	21136	41.28	31387	61.30	749	1.46
14	22253	43.46	20627	40.29	31751	62.01	748	1.46
15	21907	42.79	19772	38.62	31083	60.71	852	1.66
16	21636	42.26	19868	38.80	30520	59.61	894	1.75
17	21528	42.05	19721	38.52	30247	59.08	851	1.66
18	21160	41.33	19809	38.69	29685	57.98	876	1.71
19	21123	41.26	19603	38.29	29263	57.15	864	1.69
20	20907	40.83	19445	37.98	28730	56.11	783	1.53
21	20740	40.51	19185	37.47	28112	54.91	834	1.63
22	20114	39.29	18497	36.13	27191	53.11	951	1.86
23	19362	37.82	17657	34.49	25796	50.38	1328	2.59
24	18700	36.52	16761	32.74	24604	48.05	1443	2.82
25	16931	33.07	15145	29.58	21737	42.46	1590	3.11
26	14996	29.29	13168	25.72	18978	37.07	1281	2.50
27	13815	26.98	11440	22.34	17055	33.31	1588	3.10
28	16464	32.16	13246	25.87	20055	39.17	1210	2.36
29	21054	41.12	19387	37.87	25999	50.78	719	1.40
30	22698	44.33	21104	41.22	28299	55.27	543	1.06
31	0	0.00	0	0.00	0	0.00	0	0.00

Table 4.1

All model fields are initially interpolated spatially and temporally to each measurement ***FOV***. Cloud emissivity is then computed from (interpolated) CLW using an algorithm similar to the one used in the ECMWF operational radiation scheme (*Morcrette*, 1991b), but applied to a directional radiance instead of a flux, and incorporating the computation of layer-integrated liquid water path and corrections for multiple scattering and ice/water percentage. The effective liquid water absorption coefficient is assumed independent of frequency, as in the model radiation scheme, althought this hypothesis may introduce some systematic errors in model simulations. The layer effective cloud fraction (fraction of ***FOV*** covered by a cloud whose emissivity is unity) is then computed as the product of emissivity times cloud fraction. The vertical profile of effective cloud fraction, as seen from the top of the atmosphere (***PECF***), is needed to compute the radiance emerging from the model ***FOV***; ***PECF*** is computed using the maximum-random overlap assumption as defined by *Geleyn and Hollingsworth* (1979), in the same way as in the model radiation scheme. The summation over all model layers of ***PECF*** represents the fraction of ***FOV*** which is covered by clouds. The forward radiance model RTTOV (*Eyre*, 1991) is used to compute, in all HIRS/2 and MSU channels, the radiances in a cloudfree atmosphere and the set of overcast radiances that would be observed if a black cloud, covering the entire ***FOV***, were present at any one of the 40 pressure layers into which the atmosphere is divided for radiance computation purposes. The top temperature of the cloudy layer is assumed equal to the model temperature interpolated to the top of the layer. Since the overcast radiances are slowly varying functions of height, a linear interpolation scheme is used to compute overcast radiances at model levels (***ORM***). The knowledge of ***PECF*** and ***ORM*** allows us to compute the simulated cloudy radiance:

$$R(j) = \sum_1^N PECF(l) \cdot ORM(j,l) + SF \cdot ORM(j,0)$$

where N is the number of model layers, j is the spectral channel being simulated, ***SF*** is the fraction of ***FOV*** not covered by clouds and $ORM(j,0)$ is the radiance emitted by the underlying surface. The same linear regression described in section 2 is used to compute the simulated OLR (OLRSIM) from simulated radiances in HIRS/2 channels 2 to 8 and 9 to 12.

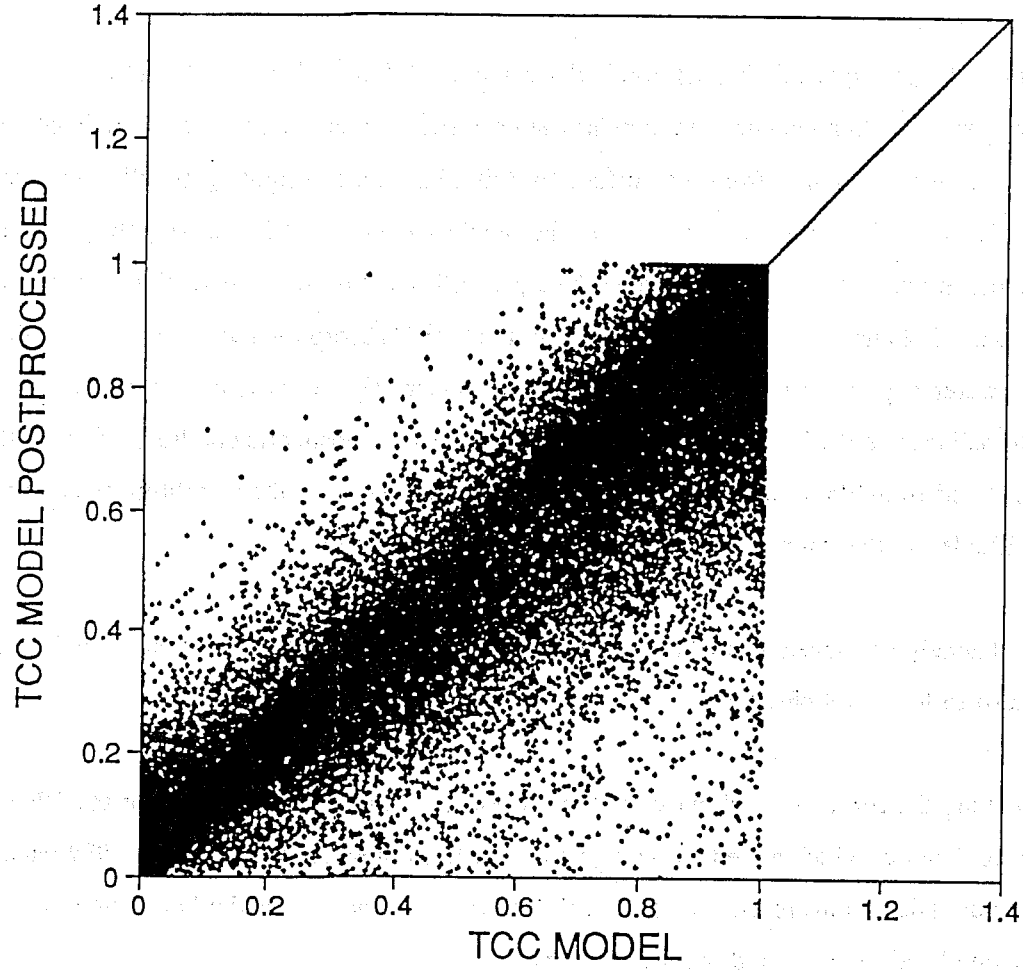

Fig 4.1 Scatter plot of Total Cloud Cover (TCC) retrieved from MARS (parameter 164) in abscissa versus TCC computed from post-processes cloud fraction and cloud liquid water.

5. RESULTS OF RADIANCE COMPARISON

Results are presented for 4 HIRS/2 channels, selected from the 24 channels of the HIRS/2-MSU system to identify the differences between the various model simulations. No microwave channels and no infrared stratospheric or high tropospheric channels are used in the comparison, since they would not show appreciable differences between the various cloud schemes, the global bias between simulations and measurements being very close to the clear bias for February 1989 and October 1993.

HIRS/2 channel 5 is a spectral channel nominally centered at 716 cm^{-1} in the 15 micron band of CO_2, and is a temperature sounding channel. In standard atmospheric conditions most of its radiance contribution comes from a layer extending from the surface to 300 hPa, with a weighting function that peaks around 600 hPa. Channel 8 is centred at 898 cm^{-1}, in the window region, and has a weighting function peaking at the surface. It was devised to determine surface properties and for cloud detection. Channels 11 and 12 are centered at 1364 and 1484 cm^{-1}, within the 6.3 microns H_2O absorption band, and were originally chosen to provide water vapour corrections for the temperature-sensing and window channels. They are both sensitive to radiance emitted by rather broad layers: in standard atmospheric conditions from 950 to 450 hPa (channel 11) and from 700 to 300 hPa (channel 12). In dry conditions the weighting functions are peaked at lower altitudes so that higher brightness temperatures are observed.

All these channels are sensitive to the presence of medium and high level clouds, while channel 8 is sensitive also to low-level cloudiness.

In the following the results for February 1989 are presented first. The discussion of the 1993 results will focus only on features which are either new or different from those shown using the 1989 data. The terms bias and standard deviation are used to indicate the mean value, and the standard deviation, of the difference between a simulated radiance and the measured value.

The effect of reducing the resolution of the measured data through filtering can be seen in Table 5.1, which shows the global bias (BIAS) and standard deviation (SD) of SPM46 for unfiltered and filtered measured brightness temperatures. The bias is below the 0.1 K level, while the reduction in standard deviation after the filtering is about 10%. Very nearly identical results are obtained for PCS forecasts and for the 1993 dataset. Since filtering of the measured radiances is based on sound principles and reduces the standard deviation, only results with filtered data will be presented hereafter.

The results of the global and zonal comparison among the SPM46 and PCS46 models are shown in Tables 5.2 and 5.3 for channel 5. Each zonal band extends 20 degrees in latitude and is centred at the value shown in the tables. The aggregate results for both satellites are shown, since the results for each satellite

are very similar both for the global and zonal statistics. The PCS46 model produces a slight reduction in bias and a slight increase in standard deviation. The clear bias (Table 2.1) is -0.15 K and the clear standard deviation is 0.75 K. PCS46 model clouds contribute a little more than 1 K to the warm bias, and about 4.7 K to the standard deviation over the sea. The zonal figures indicate that a bias reduction, going from SPM46 to PCS46, is apparent at all latitudes and that the largest contribution to the overall standard deviation comes from the latitudinal band extending from -30 degrees to 10 degrees.

		FILTERED		FULL RESOLUTION		%
CH	NTOT	BIAS	SD	BIAS	SD	
5	3867011	1.2	4.3	1.2	4.8	12
8	3867011	4.4	12.2	4.4	13.6	11
11	3867011	1.7	6.7	1.7	7.4	10
12	3867011	0.8	5.1	0.8	5.5	8

Table 5.1 Global bias and standard deviation of the differences between simulated and measured brightness temperatures. Model SPM-46. NOAA-10 and NOAA-11, 1989 dataset.

		SPM-46		PCS-46	
	NTOT	BIAS	SD	BIAS	SD
GLOBAL	3867011	1.2	4.3	1.0	4.5
LAND	1375445	1.4	3.6	1.0	3.7
SEA	2491566	1.2	4.6	1.0	4.8

Table 5.2 Global bias and standard deviation of the differences between simulated and measured brightness temperatures in HIRS/2 channel 5. NOAA-10 and NOAA-11, 1989 dataset.

		SPM-46		PCS-46	
lat	NTOT	BIAS	SD	BIAS	SD
-80.	362454	0.8	1.6	0.8	1.4
-60.	460684	0.8	2.8	0.9	2.7
-40.	432461	0.2	4.0	0.4	3.9
-20.	422530	1.8	6.7	1.1	6.9
0.	434237	2.5	6.3	2.0	7.1
20.	438607	0.3	3.3	0.2	3.8
40.	444302	1.3	3.1	1.0	3.1
60.	477017	1.9	2.7	1.6	2.8
80.	394719	1.4	2.0	1.2	1.9

Table 5.3 Zonal bias and standard deviation of the differences between simulated and measured brightness temperatures in HIRS/2 channel 5. NOAA-10 and NOAA-11, 1989 dataset, data over land and sea.

Figs 5.1a and 5.1b are bidimensional histograms of measured (filtered) channel 5 (abscissa) against the simulated value for the whole 1989 dataset. The simulations are performed using SPM46 (1a) and PCS46 (1b). The shaded portions are areas of constant density (logarithm of number of points within a 2-dimensional bin normalized to the total number of points). It is worth noting that a large portion of the data lies along the diagonal and that the scatter plot for PCS46 is more symmetrical around the diagonal than the SPM46 one, which explains the smaller overall bias at the expense of a larger standard deviation.

Tables 5.4 and 5.5 show the global and zonal distribution of bias and standard deviation for channel 8 of NOAA-11 and NOAA-10 separately. The clear bias is 0.2 K for NOAA-11 and -0.4K for NOAA-10, while the clear standard deviations are 2.8 K (NOAA-11) and 2.3 K (NOAA-10). A large bias reduction is found when using model PCS46, but the standard deviation is practically unaltered. Both models produce smaller bias and standard deviations over land than over sea, an effect particularly evident for NOAA-11. The standard deviation solely caused by clouds can be estimated over sea as about 13 K for both satellites. The zonal distribution for model PCS46 shows largest bias and standard deviation between -30 and 10 degrees, for all land and sea points and for both satellites, while a large variability in both statistics is observed for NOAA-11 over land. In addition an increase in warm bias is observed over sea towards both polar regions.

Figs 5.2a and 5.2b show the bidimensional histograms, analogous to Figs 5.1a and 5.1b, but for channel 8. There are similarities to findings for channel 5, but, in addition, there is a clear underestimation of the magnitude of the largest brightness temperature values in both models. The bidimensional histograms for PCS46 for land points (not shown) clearly show that this feature is produced by the simulations over land. Largest differences are found in the afternoon hours, monitored by NOAA-11, over desert areas; differences of up to 10-15K can often be found over large areas of the Sahara Desert (at 12 UT), the clear portions of South America (18 UT), Australia and India (06 UT). It is also found that the rate of change of brightness temperature with time, during local afternoon hours and in the morning, is slower than the one observed, indicating a phase error as well. Similar findings are also reported in *Morcrette* (1991a), where simulated brightness temperatures for the longwave channel of Meteosat are compared to reduced resolution measured data. There are several physical mechanisms that could explain the observed discrepancy. The radiance simulation could introduce errors, due to inaccurate water vapour absorption in the window region, sensed by channel 8, and to the absence of aerosol effects. However these forward simulation deficiencies cannot explain the large and extensive observed differences over the deserts, where the amount of integrated water vapour is very low. The likely explanation is that the average temperature for the first surface layer is not representative of the temperature of the first few millimetres of soil. In fact the results obtained with the 1993 dataset, discussed later, show that a change in the description of the surface physics can have considerable effects on skin temperature.

The underestimation under discussion is the cause of some of the variability noticed in zonal bias for both models. In latitude belts where large continental areas are found with low mean cloudiness the underestimation caused by a colder land surface partly compensates for the general overestimation caused by insufficient cloud development, giving rise to low bias values; in areas where cloudiness is more widespread, like the ITCZ, the bias is generally large and positive.

NOAA-11		SPM-46		PCS-46	
	NTOT	BIAS	SD	BIAS	SD
GLOBAL	1898611	4.1	12.4	2.1	12.8
LAND	672233	2.6	10.2	0.6	10.8
SEA	1226378	4.9	13.3	3.0	13.5
NOAA-10					
GLOBAL	1968400	4.7	12.1	2.8	12.3
LAND	703212	4.1	9.9	2.4	10.1
SEA	1265188	5.1	13.0	3.0	13.3

Table 5.4 Global bias and standard deviation of the differences between simulated and measured brightness temperatures in HIRS/2 channel 8 1989 dataset.

NOAA-11	ALL DATA			OVER LAND			OVER SEA		
LAT	NTOT	BIAS	SD	NTOT	BIAS	SD	NTOT	BIAS	SD
-80.	175712	2.1	6.2	131509	1.1	5.1	44203	5.0	7.9
-60.	225529	2.3	10.8	16144	3.7	6.5	209385	2.2	11.0
-40.	212448	1.7	13.0	18390	-2.2	9.5	194058	2.0	13.0
-20.	210341	2.4	17.4	48043	-1.0	19.3	162298	3.1	15.8
0.	215407	4.9	18.0	54709	4.2	19.1	160698	5.2	17.3
20.	215045	0.2	11.8	74887	-2.3	9.2	140158	1.5	12.1
40.	214483	0.3	10.9	104073	1.5	8.5	110410	1.9	11.8
60.	235032	2.0	8.9	154863	1.7	7.6	80169	2.5	10.5
80.	194614	3.8	6.6	69615	1.1	5.8	124999	5.2	6.4
NOAA-10									
-80.	186742	2.0	6.3	140249	0.9	5.2	46493	5.1	7.7
-60.	235155	2.6	10.4	16108	3.3	6.4	219047	2.5	10.6
-40.	220013	2.2	12.6	16419	2.0	9.4	203594	2.2	12.6
-20.	212189	3.3	16.8	45882	5.0	18.6	166307	2.8	15.6
0.	218830	5.6	17.5	53867	8.6	17.6	164963	4.6	16.9
20.	223562	1.9	11.2	79314	1.6	7.7	144248	2.1	12.4
40.	229819	1.8	10.3	116554	1.5	7.5	113265	2.1	12.6
60.	241985	2.4	8.3	168324	2.5	7.4	73661	2.2	10.1
80.	200105	3.9	6.2	66495	1.3	5.9	133610	5.2	5.9

Table 5.5 Zonal bias and standard deviation of the differences between simulated and measured brightness temperatures in HIRS/2 channel 8. Model PCS-46, 1989 dataset.

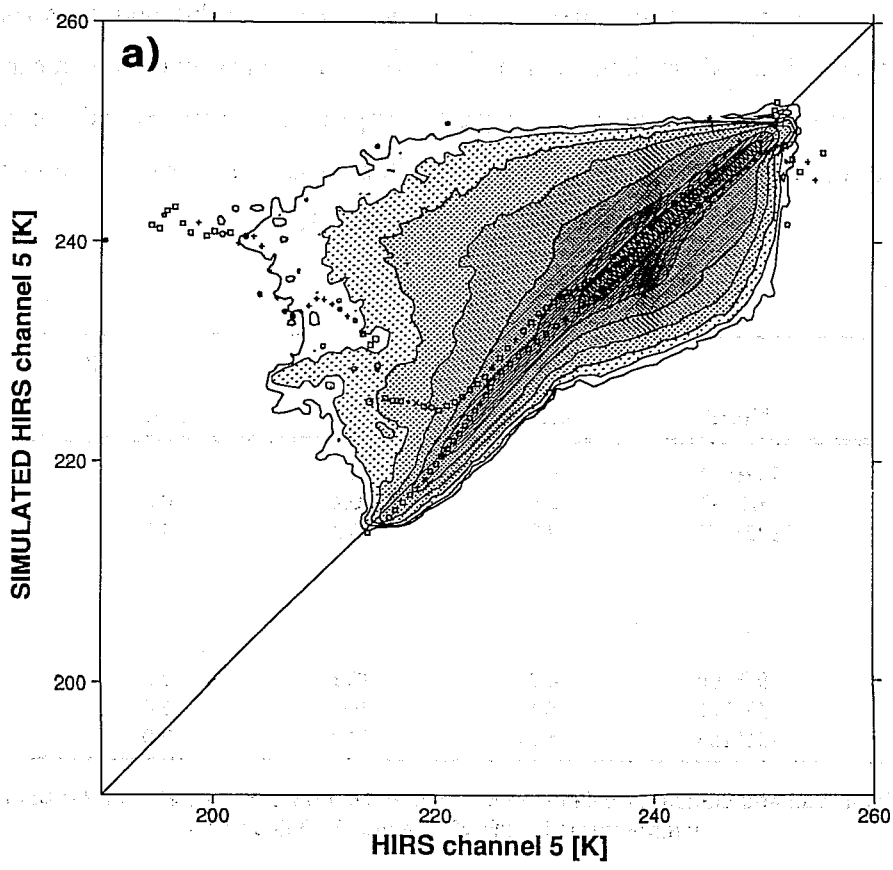

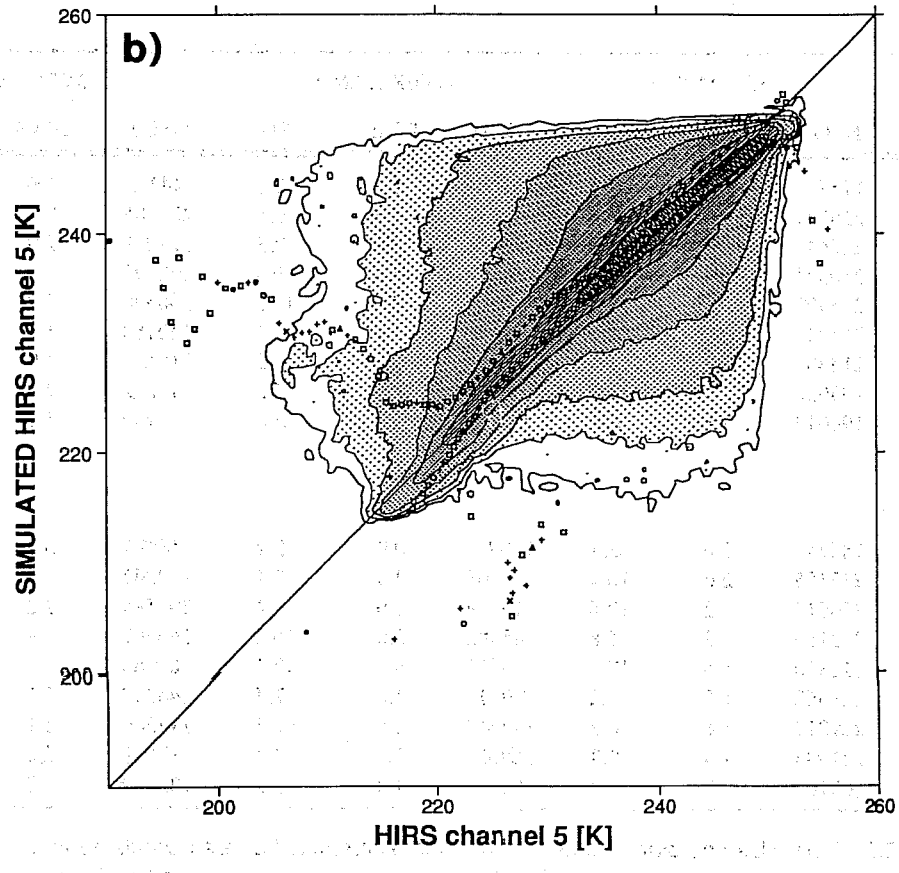

Fig 5.1 a) Bi-dimensional histogram of brightness temperature in HIRS/2 channel 5 (abscissa) versus the values simulated using the forecast model SPM46. Period: from 12UT 8 Feb. 1989 to 06UT 11 Feb. 1989. Data for the whole globe is included.

b) Same as figure 5.1a but using the forecast model PCS46.

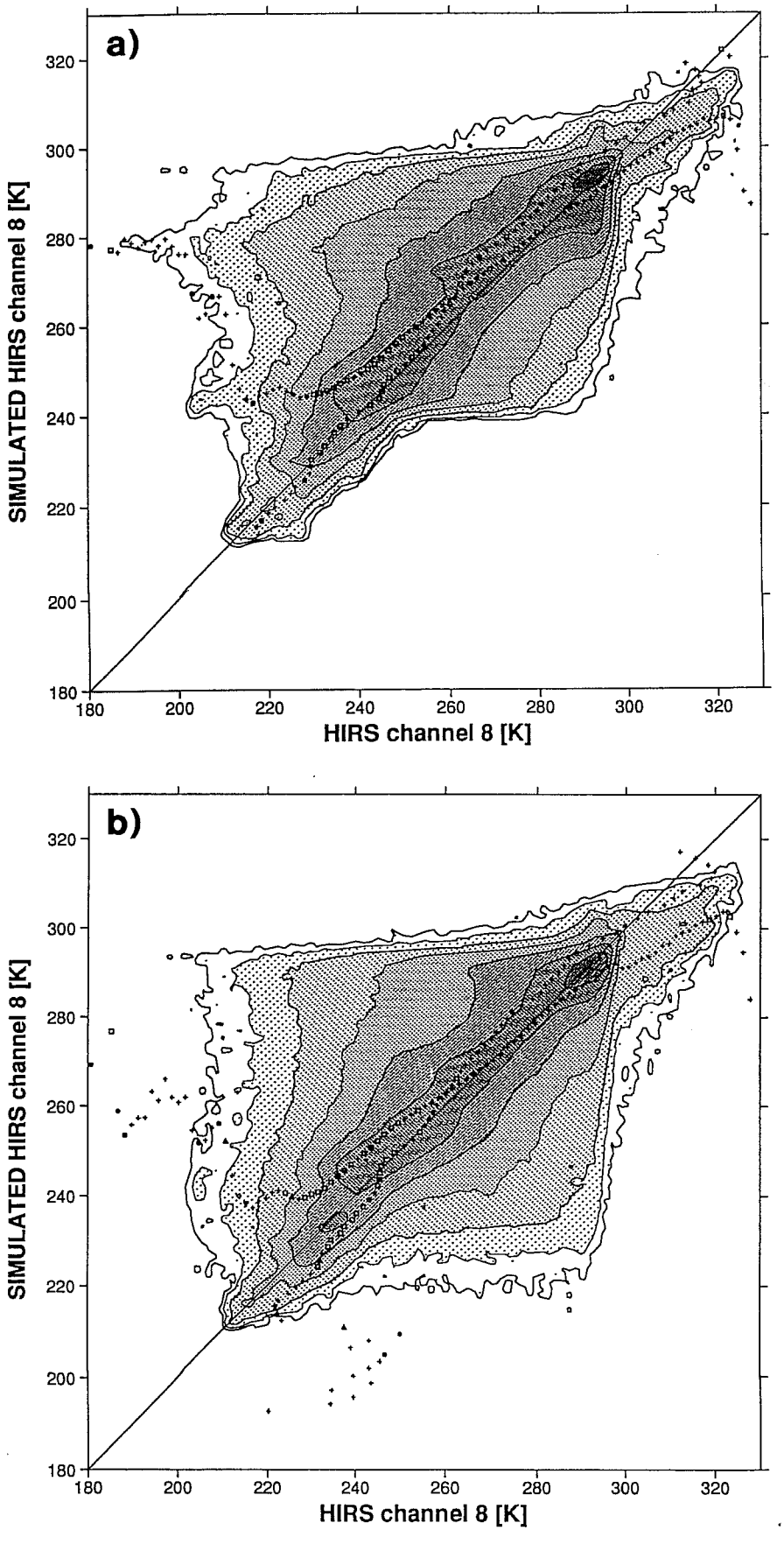

Fig 5.2 a) Bi-dimensional histogram of brightness temperature in HIRS/2 channel 8 (abscissa) versus the values simulated using the forecast model SPM46. Period: from 12UT 8 Feb. 1989 to 06UT 11 Feb. 1989. Data for the whole globe is included.

b) Same as figure 5.2a but using the forecast model PCS46.

The larger asymmetry of the scatter in the mid portion of the plot for SMP46, when compared to PCS46, is due to measured values in channel 8 reaching values as low as 200 K, while the lowest values from SPM46 are about 240 K. The same effect was seen for channel 5 (Figs 5.1a and 5.1b). A similar problem is reported by *Morcrette* (1991a). These large differences are attributable both to inaccurate physics and circulation patterns. A symmetric (however spread) scatter is in fact a necessary, but not sufficient, condition to consider the physical parametrizations as adequate, the scatter being then due mostly to positional errors in the circulation pattern. By physical parametrization here it is meant those processes which have some impact on the radiance fields of channel 5 and 8, and, as we will see, channel 11 and 12. After examining individual six-hourly scatter plots (not shown) it is found that most of the asymmetry for SPM46 originates from data in the latitude belt from 30 to 10 degrees south, where the ITCZ is found at this time of the year.

The large warm bias in the Arctic and in the Antarctic region over sea can have a number of causes. No forward model bias correction scheme is applied in the present dataset, but the magnitude of the clear bias (over sea) is less than 0.3 K in both polar regions for the period under consideration. There may also be differences in the structure of model clouds, with respect to the real arctic clouds, and in the model surface temperature, in the presence of extremely cold sea ice, which may be different from the actual temperature. The bidimensional histogram of channel 8 brightness temperatures, for the latitude band from 70 to 90 degrees South (not shown), indicates that the core of the simulated values is offset, while some spread is probably caused by clouds; therefore model ice surface temperature is the main reason for the observed warm bias, a result reported also in *Morcrette* (1991a). Nearly the same problem is found over sea in the latitude region from 70 to 90 degrees North.

The images of Figs 5.3 to 5.5 show the geographical distribution respectively of the measured channel 8 (Fig 5.3), of the simulated data using SPM46 (Fig 5.4) and of PCS46 (Fig 5.5), for a six hour period centred at 12UT of 8 February 1989. All the images use the same colour code. The measured data clearly show the Sahara region, with its large brightess temperature, and the location of the ITCZ in the Indian and Pacific oceans slightly south of the Equator. The largest and most obvious differences, between simulations and measurements, and between each model, are displayed in the ITCZ area, and are related to convective activity.

The two models produce quite a different geographical distribution of the brightness temperature, both in the tropics and at mid-latitude. In the tropical region SPM46 provides a fair description of the area spread of the organized convection, but it severely overestimates the measured brightness temperature in channel 8; differences of 30 K are found in deep convection areas, over oceans and over land. In experiment PCS46 much lower brightness temperatures are found in active convective areas, a far better match to the

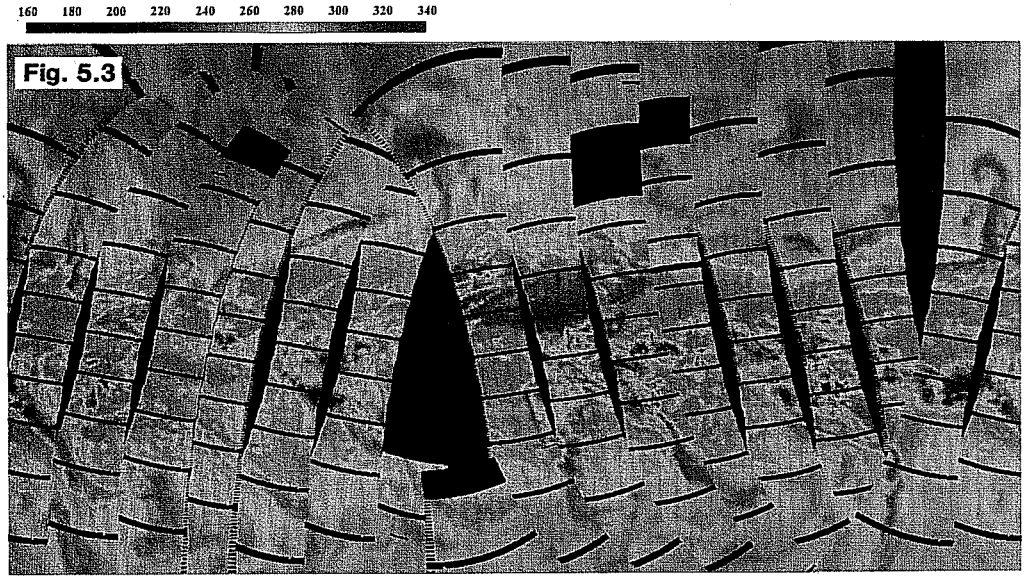

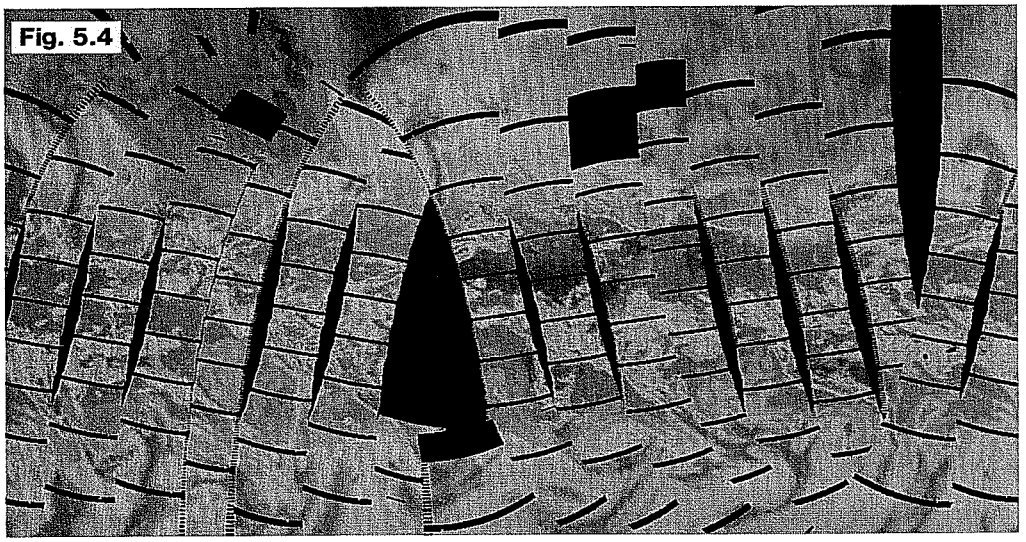

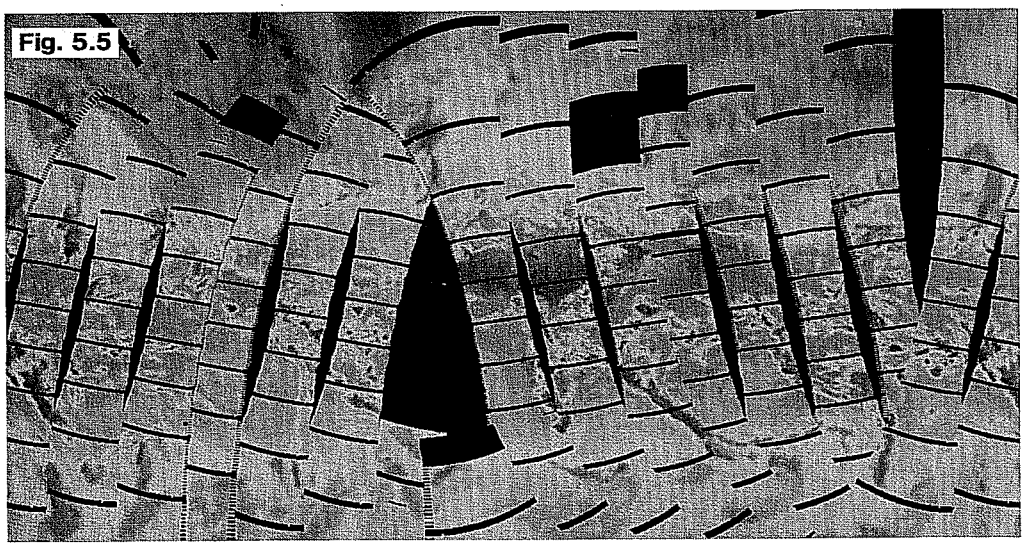

Fig 5.3 Measured HIRS/2 channel 8 for a six-hour period centred at 12UT, 8 Feb. 1989. The data, measured by both NOAA-10 and NOAA-11, is displayed in Mercator projection and is colour coded in the range 160 K (navy blue) to 340 K (purple). Black points indicate locations where data is missing (calibration cycle, data parity error or data outside the six-hour window).

Fig 5.4 Same as figure 5.3 but for simulated channel 8 from SPM46.

Fig 5.5 Same as figure 5.3 but for simulated channel 8 from PCS46.

measurements, but the cloudy structures responsible for it are isolated and cover only a fraction of the convective regions that can be inferred from measurements. There are large areas in SPM46, where the surface emission is shielded by cloudy structures, that are nearly free of clouds in PCS46. Since the SPM46 convective cloud scheme generates, in the tropics, low and middle level cloudiness whose fractional cover is higher than in PCS46, and a high level cloudiness which is comparable (albeit slightly larger) to PCS46, the observed differences are principally due to the amount of cloud liquid water, and therefore to the cloud layer emissivity, that each model generates.

In mid-latitudes, low and mid level cloudiness (cloud fraction) is much higher and more widespread in PCS46, while SPM46 has more high-level cloudiness. As noted already for the tropical region, both models overestimate cloud top temperatures in strong convective areas: however strong frontal regions are better described by PCS46, while more moderate fronts are better described by SPM46. In the regions behind cold fronts the brightness temperatures predicted by SPM46 are consistently warmer than PCS46, an effect that seems linked to the lower amount of low and middle level cloudiness generated by SPM46. One must remember however that some of the differences, between measurements and simulations, are due to the use of fields of cloud fraction and cloud liquid water which differ to some extent from the fields generated by the forecast model, as discussed in section 4.

Tables 5.6 and 5.7 show the global bias and standard deviation for SPM46 and PCS46, for channel 11 and channel 12 respectively. Figs 5.6a and 5.6b show the zonal bias (a) and standard deviation (b) in channel 11 of NOAA-10; the thin line is the clear bias (standard deviation); the dashed line is the bias (standard deviation) from simulations over sea using SPM46; and the wide line is the bias (standard deviation) from simulations over sea using PCS46. Figs 5.7a and 5.7b are analogous to Figs 5.6a and 5.6b respectively, but are computed for channel 12.

NOAA-11		SPM-46		PCS-46	
	NTOT	BIAS	SD	BIAS	SD
GLOBAL	1898611	1.5	6.8	1.4	7.0
LAND	672233	1.5	5.5	1.1	5.7
SEA	1226378	1.5	7.4	1.4	7.5
NOAA-10					
GLOBAL	1968400	1.8	6.7	1.7	6.9
LAND	703212	2.0	5.5	1.7	5.6
SEA	1265188	1.8	7.2	1.7	7.4

Table 5.6 Global bias and standard deviation of the differences between simulated and measured brightness temperatures in HIRS/2 channel 11. 1989 dataset.

NOAA-11		SPM-46		PCS-46	
	NTOT	BIAS	SD	BIAS	SD
GLOBAL	1898611	0.6	5.1	1.4	7.0
LAND	672233	1.1	4.2	1.1	5.7
SEA	1226378	0.4	5.5	1.4	7.5
NOAA-10					
GLOBAL	1968400	0.9	5.1	1.2	5.3
LAND	703212	1.4	4.2	1.5	4.3
SEA	1265188	0.7	5.5	1.1	5.7

Table 5.7 Global bias and standard deviation of the differences between simulated and measured brightness temperatures in HIRS/2 channel 12. 1989 dataset.

Results for channel 11 suggest that there is only a slight difference between the results of the two models. The pattern in all the curves in Fig 5.6 is similar: positive biases outside the tropical area, and smaller (or negative) bias in the tropical region, where the standard deviation attains its largest values. Comparing the bias values for the clear case and model PCS46, the effect of cloudiness amounts to about 1.5 K outside the tropics, increasing to 2.5 K between -30 and 10 degrees. The only region where model PCS46 compares less favourably to measured data than SPM46 is between -90 and -70 degrees. Similar results are found also for data measured by NOAA-11. Results for channel 12 indicate that PCS46 produces a larger bias and a larger standard deviation, both globally and zonally, particularly between -90 and -50 degree latitude. The structure of zonal bias of SPM46 and PCS46 is similar to the clear case, but PCS46 produces a drier upper troposphere than SPM46. It is however extremely difficult to separate the effects caused by the water vapour field and cloudiness. An automatic method, to identify clear FOVs and to compare their radiances to clear model radiances, is required to separate clouds from water vapour features. However inspection at images, like the one shown in Figs 5.3 to 5.5, of measured and simulated radiances in water vapour channels, may reveal interesting features. For example, in both channels, but expecially in the lower tropospheric channel (11), the observed subtropical dry regions are generally drier than simulations in all experiments. This evidence, together with the weaker convective activity in the ITCZ, a feature common to a various degree to all the forecasts, may be explained as the result of a weak Hadley circulation, which may be partly due to the 1989 operational analysis used as a starting point for all the forecasts. In May 1989 the *Kuo* (1974) convection scheme was replaced by the mass flux scheme of *Tiedtke* (1989), resulting in a sizeable increase of the intensity of the Hadley circulation.

Table 5.8 shows the global bias and standard deviation in channels 5 and 8 for the 1993 dataset. The changes from SPM46 (and 1989 operational analysis) to SPM48 (and 1993 operational analysis) produce a halving of bias with no changes to standard deviations in channel 5, while hardly any change is seen in channel 8. The fit produced by PCS48 is globally better, both in channel 5 and 8, than SPM48. The zonal statistics for channel 8 shows a 4K warm bias and 20K standard deviation in the equatorial region, where

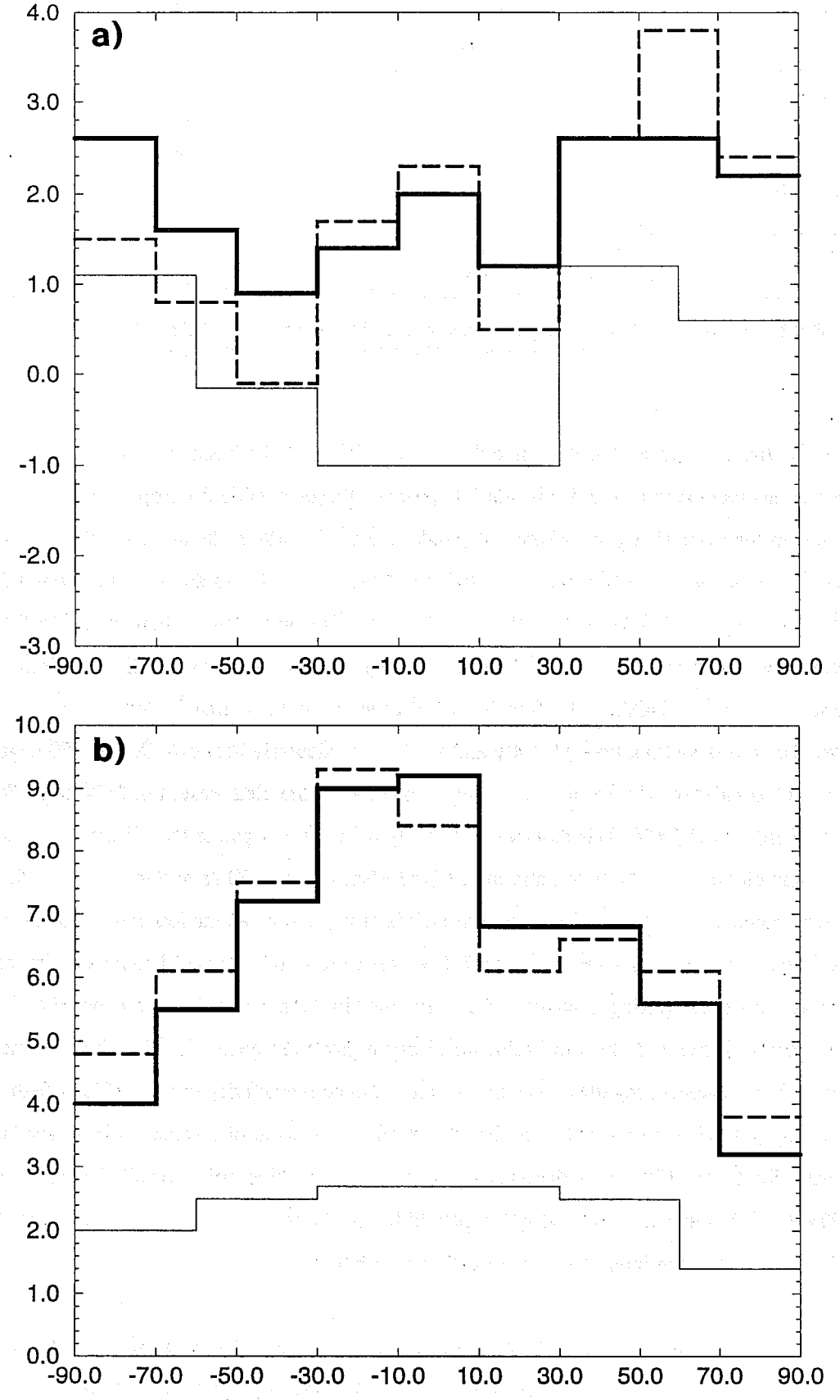

Fig 5.6a Zonal mean difference between simulations and measured brightness temperature in HIRS/2 channel 11 of NOAA-10. Thin line is clear bias, wider line is simulations based on model PCS46, dashed line is simulations based on SPM46.

Fig 5.6b Zonal standard deviation of the difference between simulations and measured brightness temperature in HIRS/2 channel 11 of NOAA-10. Thin line is clear bias, wider line is simulattions based on model PCS46, dashed line is simulations based on SPM46.

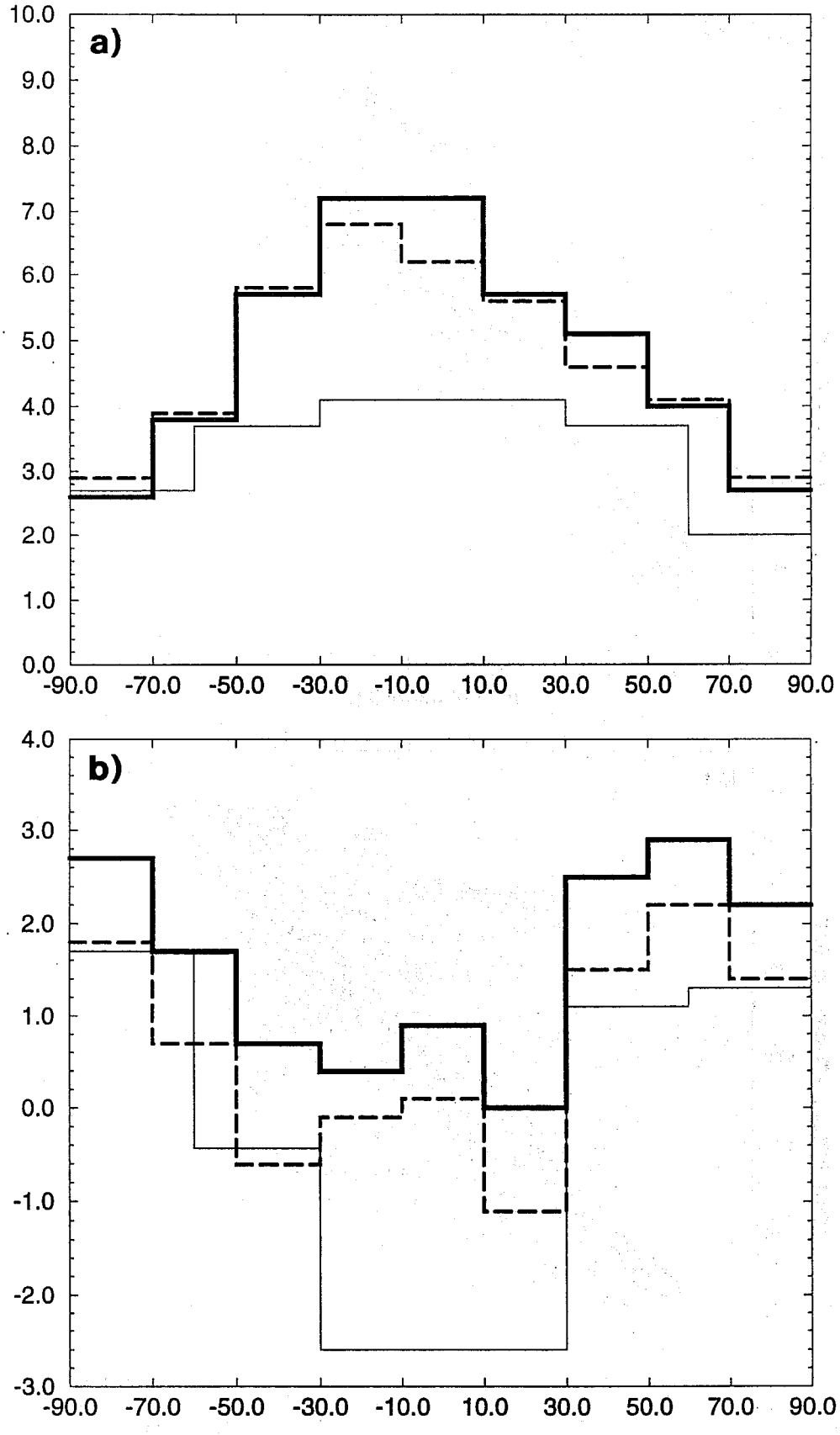

Fig 5.7 a) Same as figure 5.6a but for HIRS/2 channel 12.
b) Same as figure 5.6b but for HIRS/2 channel 12.

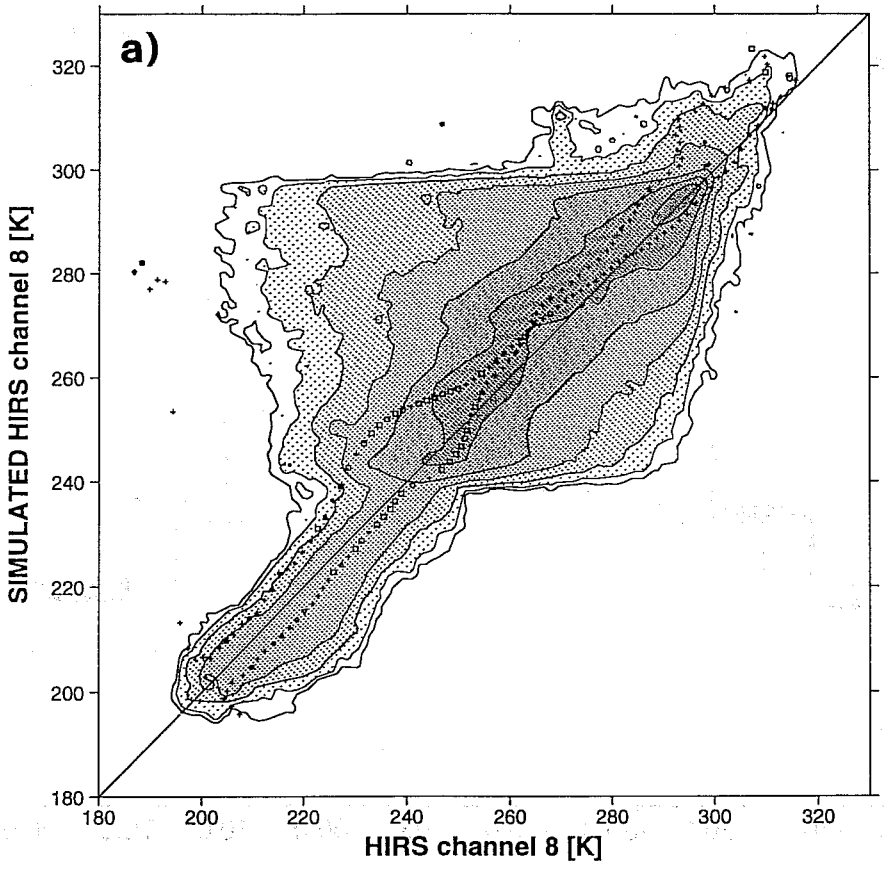

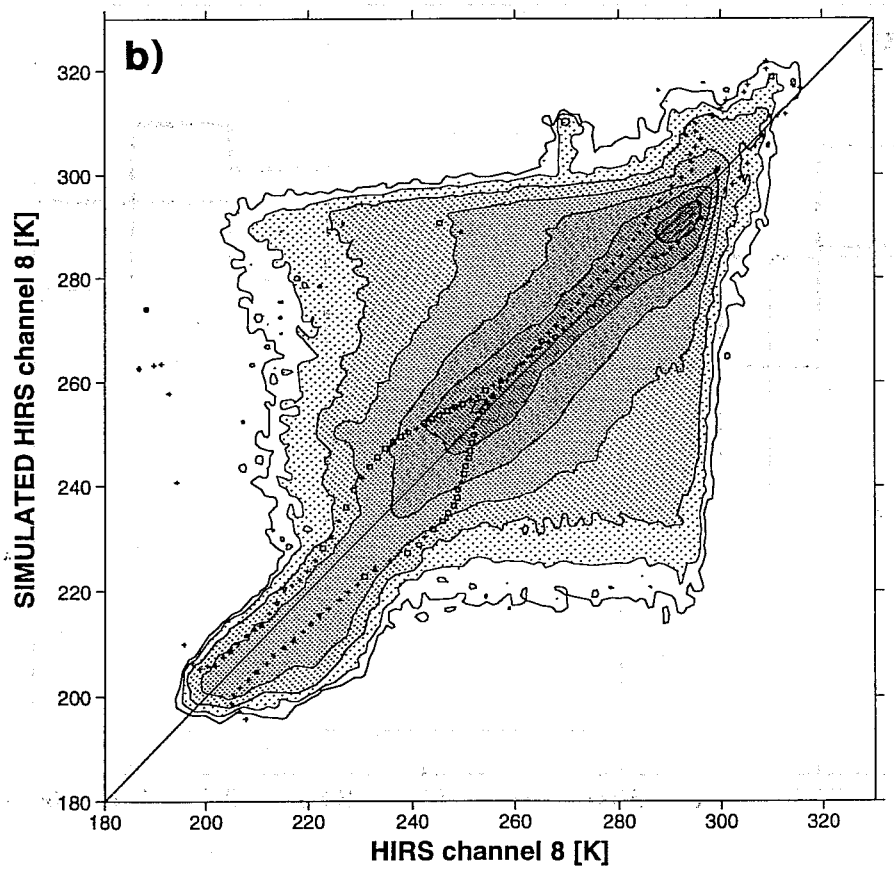

Fig 5.8 a) Bi-dimensional histogram of brightness temperature in HIRS/2 channel 8 (abscissa) versus the values simulated using the forecast model SPM48. Period: from 00UT 14 October 1993 to 06UT 16 October 1993. Data for the whole globe is included.

b) Same as figure 5.9a but using the forecast model PCS48.

the ITCZ, less developed than the one observed in 1989, is located. Figs 5.8a and 5.8b are the bidimensional histograms of measured channel 8 brightness temperature versus simulations using SPM48 (a) and PCS48 (b). The two distributions possess many of the features already noted for the 1989 dataset, except that a warm bias is now apparent in the upper part of the plot, which corresponds to emission from deserts in clear sky conditions. The new surface physics, introduced in cycle 48, produces brightness temperatures in the window channel which are too high by 5 to 8 degrees during the afternoon hours, and too low by up to 5 degrees in early morning. No data are available for the warmest hours of the day.

		HIRS2/CHANNEL 5				HIRS/2 CHANNEL 8			
		SPM-48		PCS-48		SPM-48		PCS-48	
	NTOT	BIAS	SD	BIAS	SD	BIAS	SD	BIAS	SD
GLOBAL	2539146	0.6	4.5	0.1	4.7	4.2	12.7	1.5	12.8
LAND	909591	0.4	4.5	0.0	4.5	2.8	12.0	1.0	12.0
SEA	1629555	0.7	4.5	0.2	4.8	5.0	12.8	1.8	13.1

Table 5.8 Global bias and standard deviation of the differences between simulated and measured brightness temperatures in HIRS/2 channels 5 and 8. NOAA-11 and NOAA-12, 1993 dataset.

6. RESULTS OF COMPARISON OF LONGWAVE FLUXES AT TOP OF ATMOSPHERE

As explained in sections 2 and 4, three estimates of OLR are produced: OLR derived from HIRS/2 radiance measurements (OLRTOV), OLR derived from simulated HIRS/2 radiances (OLRSIM) and OLR generated by the forecast model (OLRMOD). Deriving an estimate of OLR from the measured and simulated radiances is about the only way to compare the model radiative flux scheme with the radiation scheme used for the present simulations.

Most of the findings described previously, when discussing the 1989 dataset, also show on the OLR distribution. They will only be listed in the following:

i. The global bias between OLRSIM and OLRTOV, computed using PCS46, is much reduced with respect to SPM46, while the magnitude of the standard deviation increases (see Table 6.1). This result is consistent with the findings of the preceding section.

ii. OLRSIM overestimates OLRTOV by as much as 60-100 Wm^{-2} in deep convection areas, over the oceans and over land, both in the tropical region and at mid latitudes.

iii. OLRSIM underestimates the OLRTOV field (in the 1989 dataset), by as much as 40 Wm^{-2}, in early afternoon over deserts in clear sky conditions in both the SPM46 and PCS46 models. A phase error

in the temporal variation of OLR over land is also observed in both models, mostly caused by the phase error already discussed for channel 8. The surface scheme, introduced in SPM48 and PCS48, produces an OLRSIM warm bias in the same areas around 16:00 local time (up to 35 Wm^{-2}), and a cold bias (up to -20 Wm^{-2}) around 4:00. The effect is still quite large after taking into account the expected OLR bias for NOAA-11 mentioned in section 2.

iv. A large warm bias between OLRSIM and OLRTOV is observed in both polar regions over sea in the 1989 dataset. Examination of brightness temperatures in HIRS/2 channel 8 have indicated that the likely cause of the bias is a too high model surface temperature over ice.

NOAA-11		SPM:SIM-TOV		SPM:MOD-TOV		PCS:SIM-TOV		PCS:MOD-TOV	
	NTOT	BIAS	SD	BIAS	SD	BIAS	SD	BIAS	SD
GLOBAL	1898598	14.9	30.4	10.8	31.2	8.2	31.0	8.8	32.8
LAND	672230	8.7	26.4	10.5	27.7	2.7	27.9	8.9	28.2
SEA	1226368	18.3	31.7	11.0	32.6	11.2	31.7	8.8	34.8
NOAA-10									
GLOBAL	1968397	9.2	29.0	11.7	30.5	3.4	29.0	9.2	32.1
LAND	703211	8.4	23.3	16.1	24.2	3.9	23.7	13.3	24.4
SEA	1265186	9.6	31.4	9.3	33.1	3.1	31.3	6.9	35.2

Table 6.1 Global bias and standard deviation of the differences between OLRSIM, OLRMOD and OLRTOV (Wm-2). Filtered HIRS/2 data. Model: SPM46 (SPM) and PCS46 (PCS). 1989 dataset.

The discussion of the differences between OLRSIM and OLRTOV is applicable to a large extent also to the differences found when comparing OLRMOD versus OLRTOV. As seen in Table 6.1, the OLRMOD values from PCS46 generally produce a better fit to the data in terms of bias, albeit an increase in standard deviation. A similar finding was already noted when discussing the radiance data. Zonal statistics are shown in Table 6.2 for both models. Images which display the geographical distribution of OLRMOD (not shown) enable one to address further the differences between the two fields. The main findings are:

a. in the latitude band from 30N to 30S in cloudfree areas OLRMOD is clearly higher than OLRSIM (and OLRTOV) by 20 to 50 Wm^{-2};

b. a large warm bias is seen in both polar regions over land with PCS46; this is not so evident when comparing the OLRSIM data to OLRTOV;

c. OLRMOD attains lower values in areas of deep convection, which are more widespread both in the tropical and mid-latitude regions.

These differences do not yet have a clear-cut explanation. In section 4 the effect of spectral truncation has been discussed. The computation of OLRSIM uses a spectrally-truncated representation of the grid point values of cloud fraction and cloud liquid water used within the forecast model's runs. We consider this difference responsible for a large part of the disagreement listed in c. The different behaviour described under a. and b. will however require further investigation.

		ZONAL OVER LAND				ZONAL OVER SEA				
		SPM-46		PCS-46			SPM-46		PCS-46	
LAT	NTOT	BIAS	SD	BIAS	SD	NTOT	BIAS	SD	BIAS	SD
-80.	271757	17.8	14.4	16.4	12.2	90696	6.7	22.1	11.0	19.8
-60.	32252	5.5	16.3	9.0	15.4	428429	4.0	27.4	2.4	26.1
-40.	34809	0.5	26.6	1.2	25.5	397652	8.2	33.3	9.1	33.3
-20.	93925	15.0	42.6	4.6	46.1	328602	13.3	38.2	9.4	40.9
0.0	108575	23.0	39.9	13.5	45.0	325658	12.7	39.1	7.8	46.5
20.0	154201	14.8	26.3	14.1	25.8	284404	15.4	33.4	14.3	34.3
40.0	220627	11.0	20.6	9.2	20.5	223675	9.0	30.8	2.5	30.4
60.0	232185	7.5	18.5	7.7	18.3	153829	3.7	24.8	-4.0	26.1
80.0	136110	16.9	15.1	14.7	14.3	258609	15.8	18.0	16.5	18.3

Table 6.2 Zonal bias and standard deviation of the differences between OLRMOD and OLRTOV (Wm-2). Data for NOAA-11 and NOAA-10. 1989 dataset.

7. CONCLUSIONS

About six days of raw HIRS/2 and MSU radiance data have been processed with the aim of understanding to what extent simulated raw radiances, computed from the early stages of a forecast model, compare to the measured values. This diagnostic step allows a detailed examination of aspects of the hydrological cycle and energetics that may need to be improved at ECMWF to make the assimilation of raw radiances feasible.

Two datasets were employed: three days of global data in February 1989 and three days in October 1993. A number of forecast experiments were run, involving four different versions of the forecast model: the operational spectral model (SPM) cycle 46 and cycle 48, and the Prognostic Cloud Scheme (PCS) applied to both the SPM cycles. The cycle 46 experiments are compared to the 1989 data, while the cycle 48 experiments are used in the diagnostic study for 1993.

Radiance simulations are based on model fields obtained from a short-range (24 to 48 hours) forecast so that spin-up effect are mostly avoided and the description of the dynamical fields is still accurate. The

simulations involve cloud parameters, cloud fraction and cloud liquid water. For the present exercise the radiative properties of clouds are computed as in the operational radiation scheme.

The resolution of HIRS/2 measurements is about 40 km and therefore higher than the model resolution, which can be estimated at about 80 to 90 km. To reduce the effect of sub-grid scale processes present in the measurements, each orbit radiance field and OLR field has been filtered using a bi-dimensional gaussian filtering function to reduce the resolution to a figure similar to the model's.

Four HIRS/2 channels are used in the comparison: channel 5, a temperature sounding channel whose weighting function peaks at about 600 hPa; channel 8, a window channel devised to determine surface properties and for cloud detection; and channels 11 and 12, which measure the water vapour emission in the low and middle troposphere. All these channels are sensitive to the presence of medium and high level clouds while channel 8 is sensitive also to low-level cloudiness.

Estimates of OLR obtained from the measured (OLRTOV) and from the simulated radiances (OLRSIM), using the same statistical regression, are compared with each other and with the OLR computed by the forecast model (OLRMOD). The OLR comparison gives an indication of the energy involved when analysing differences observed in the radiance fields; moreover it allows to compare the forecast model radiative flux scheme to the radiation scheme used for the radiance simulations.

From the detailed discussion of section 5, the following points emerge:

i. Model PCS (both cycle 46 and 48) generally produces a decrease in the magnitude of the global bias in channel 5 and 8, and in the OLR. The decrease is evident at all latitudes. The standard deviation is slightly larger in experiment PCS; since the PCS model shows a definite improvement in the description of the radiance field in presence of deep clouds, the increase in standard deviation is likely due to the increased radiance range in the presence of circulation errors whose magnitude is similar in both models. The largest contribution to the global standard deviation comes, in all experiments, from the latitudinal band where the ITCZ is located.

ii. The two models produce quite a different geographical distribution of the brightness temperature and OLR fields, both in the tropics and at mid-latitude. In the tropical region SPM provides a fair description of the area spread of the organized convection, but it severely overestimates the measured brightness temperature, at all channels sensitive to clouds, and the OLR; PCS produces much lower radiance and OLR values in strong convective areas, a far better match to the measurements, but the convective activity covers only a fraction of the convective regions that can

be inferred from measurements. These observed differences are principally due to the amount of cloud liquid water, and therefore to the cloud layer emissivity, that each model generates. At mid-latitude, low- and mid-level cloud fraction is higher and more widespread in PCS, while SPM46 has more high-level cloudiness. Both models overestimate cloud top temperatures in strong convective areas, but strong frontal regions are better described by PCS46, while more moderate fronts are better described by SPM. The brightness temperatures predicted by SPM are consistently warmer than PCS behind cold fronts, an effect that seems linked to the lower amount of low- and mid-level cloudiness generated by SPM46.

iii. The 1989 dataset shows that both models clearly underestimate the brightness temperature of channel 8 over desert areas, in clear sky conditions, by up to 10-15 K and of OLR by 30-40 Wm^{-2}, since the average temperature of the surface layer is not representative of the radiative temperature of the soil. It is also found that the rate of change of brightness temperature with time, during local afternoon hours and in the early morning hours, is smaller than the one observed, indicating a phase error as well. The changes in the parametrization of surface processes, introduced with cycle 48 and examined with the 1993 dataset, produce brightness temperatures warmer than the measured values by about 5 to 8 K during the afternoon hours, and colder by up to 5 K in early morning.

iv. A warm bias is produced by the two models over both polar regions over sea, in both datasets, likely caused by model ice temperatures being several degrees too warm.

v. Results for water vapour channel 11 suggest only a slight difference between the results of the two models. Instead PCS produces a larger warm bias and a larger standard deviation than SPM in channel 12, both on a global and zonal basis; this can be interpreted as PCS producing a dryer mid and upper troposphere. In the 1989 dataset the observed subtropical dry and cloudfree regions are generally dryer than simulations in all experiments. This evidence, together with the weaker convective activity in the ITCZ, a feature common to a various degree to all the forecasts, may be explained as the result of a weak Hadley circulation, which may in turn partly be due to the 1989 operational analysis used as a starting point for both experiments. It is, however, generally very difficult to distinguish water vapour effects in the presence of clouds, since these have a considerable effect even in channel 12.

vi. The differences observed between OLRMOD and OLRTOV are similar to those found when comparing OLRSIM and OLRTOV. In addition it is found that:

a) in the tropical region, in cloudfree areas, OLRMOD is clearly higher than OLRSIM and OLRTOV by 20 to 50 Wm^{-2};

b) a large warm bias is seen in both the polar regions over land with PCS46, not so evident when comparing the OLRSIM data to OLRTOV;

c) OLRMOD attains lower values in areas of deep convection, which are more widespread both in the tropical and mid-latitude regions.

We believe that problem c) is mostly caused by differences induced by the postprocessing of cloud parameters discussed in section 4. The differences listed under a) and b) do not yet have a clear cut explanation.

These results are not to be considered exhaustive of the information which the data contain. The same analysis methods can be applied to specific areas to verify the ability of the model in different surface and atmospheric (including cloud) conditions. The inclusion of a cloud detection scheme will allow comparison of measured clear and cloudy radiances with the model equivalents, found at the same or nearby fields of view. Moreover the information contained in the set of HIRS/2 and MSU radiances has not yet been fully exploited. It already shows, however, the potential of directly comparing raw radiance measurements to simulations based on model fields.

8. REFERENCES

Amato, U, V Cuomo, G Pavese, R Rizzi, C Serio and V Tramutoli, 1991: Cloud clearing with radial basis functions. Technical Proceedings of the Sixth International TOVS Study Conference, May 1-6, available from CIMSS Wisconsin.

Betts, A K, J H Ball and A C M Beljaars, 1993: Comparison between the land surface response of the European Centre Model and the FIFE-1987 data. Submitted to Q J R Meteorol Soc

Browning, K A, 1994: Survey of perceived priority issues in the parametrization of cloud-related processes in GCMs. Q J R Meteorol Soc, 120, 483-487.

Ellingson, R G, D J Yanuk, Hai-Tien Lee and A Gruber, 1989: A technique for estimating outgoing longwave radiation from HIRS radiance observations, J Atmos Ocean Techn, 6, 706-711.

Ellingson, R G, Hai-Tien Lee and A Gruber, 1990: Validation of a technique for estimating outgoing longwave radiation from HIRS radiance observations, Seventh American Meteorological Society Conference on Atmospheric Radiation, July 23-27, San Francisco, California.

Eyre, J R, 1991: A fast radiative transfer model for satellite sounding systems. ECMWF Research Department Technical Memorandum No. 176, March.

Eyre, J R, 1992: A bias correction scheme for simulated TOVS brightness temperatures. ECMWF Research Department Technical Memorandum No. 186, October.

Eyre, J R, G A Kelly, A P McNally, E Andersson and A Persson, 1993: Assimilation of TOVS radiance information through one-dimensional variational analysis. Q J R Meteorol Soc, 119, 1427-1463.

Geleyn, J-F and A Hollingsworth, 1979: An economical analytical method for the computation of the interaction between scattering and line absorption of radiatio. Beitr Phys Atmos, 52, 1-16.

Hamill, T M, R P d'Entremont and J T Bunting, 1992: A description of the Air Force real time nephanalysis model. Wea Forecasting, 7, 288-306.

Heymsfield, A J and L J Donner, 1990: A scheme for parametrizing ice-cloud water content in general circulation models. J Atmos Sci, 47, 1865-1877.

Hou Yu-Tai, K A Campana, K E Mitchell, S-K Yang and L L Stowe, 1993: Comparison of an experimental NOAA AVHRR cloud dataset with other observed and forecast cloud datasets. J Atmos Oceanic Techn, 10, 833-849.

Kuo, H L, 1974: Further studies of the parametrization of the influence of cumulus convection of large scale flow. J Atmos Sci, 31, 1232-1240.

Miller, M, A C M Beljaars and T N Palmer, 1991: The sensitivity of the ECMWF model to the parametrization of evaporation from tropical oceans. J Clim, 5, 418-434.

Morcrette, J-J, 1991: Evaluation of model generated cloudiness: satellite observed and model generated diurnal variability of brightness temperature. Mon Wea Rev, 119, 1205-1224.

Morcrette, J-J, 1991: Radiation and cloud radiative properties in the ECMWF operational weather forecast model. J Geo Res, 96D, 9121-9132.

Ritter, B, 1992: Validation of radiation and clouds. Proceedings of ECMWF Seminar on Validation of Models over Europe, 7-11 September, 227-264.

Rossow, W B and R A Schiffer, 1991: ISCCP cloud data products. Bull Amer Meteor Soc, 72, 2-19.

Slingo, J M, 1987: The development and verification of a cloud prediction scheme for the ECMWF model. Q J R Meteorol Soc, 113, 899-927.

Slingo, A and J M Slingo, 1988: The response of a general circulation model to cloud longwave radiative forcing. I: Introduction and initial experiments. Q J R Meteorol Soc, 114, 1027-1062.

Smith, W L, 1979: H M Woolf, C M Hayden, D Q Wark and L M McMillin, The TIROS-N operational vertical sounder. Bull Amer Meteorol Soc, 60, 1177-1187.

Smith, W L and H M Woolf, 1983: Geostationary satellite sounder (VAS) observations of longwave radiation flux. Proc. of the Conference on Satellite Systems to Measure Radiation Budget Parameters and Climate Change Signals, Igls, Austria, 29 August - 2 September.

Smith, W L, H M Woolf, S J Nieman and T H Achtor, 1993: ITPP-5 - the use of AVHRR and TOGR in TOVS data processing. Technical Proceedings of the Seventh International TOVS Study Conference, Igls, 10-16 February 1993, edited by J R Eyre, ECMWF.

Stowe, L L, E P McClain, R Carey, P Pellegrino, G Gutman, P Davis, C Long and S Hart, 1991: Global distribution of cloud cover derived from NOAA/AVHRR operational satellite data. Adv Space Res, 11, 51-54.

Tiedtke, M, 1989: A comprehensive mass-flux scheme for cumulus parametrization in large scale models. Mon Wea Rev, 117, 1779-1800.

Tiedtke, M, 1993: Representation of clouds in large-scale models. Mon Wea Rev, 121, 3040-3061.

LIST OF ECMWF TECHNICAL REPORTS

1	A case study of a ten day forecast. (1976)	Arpe, K., L. Bengtsson, A. Hollingsworth, and Z. Janjić
2	The effect of arithmetic precision on some meteorological integrations. (1976)	Baede, A.P.M., D. Dent, and A. Hollingsworth
3	Mixed-radix Fourier transforms without reordering. (1977)	Temperton, C.
4	A model for medium range weather forecasts - adiabatic formulation. (1977)	Burridge, D.M., and J. Haseler
5	A study of some parameterisations of sub-grid processes in a baroclinic wave in a two dimensional model. (1977)	Hollingsworth, A.
6	The ECMWF analysis and data assimilation scheme: analysis of mass and wind field. (1977)	Lorenc, I. Rutherford and G. Larsen
7	A ten-day high-resolution non-adiabatic spectral integration; a comparative study. (1977)	Baede, A.P.M., and A.W. Hansen
8	On the asymptotic behaviour of simple stochastic-dynamic systems. (1977)	Wiin-Nielsen, A.
9	On balance requirements as initial conditions. (1978)	Wiin-Nielsen, A.
10	ECMWF model parameterisation of sub-grid scale processes. (1979)	Tiedtke, M., J.-F. Geleyn, A. Hollingsworth, and J.-F. Louis
11	Normal mode initialization for a multi-level grid-point model. (1979)	Temperton, C., and D.L. Williamson
12	Data assimilation experiments. (1978)	Seaman, R.
13	Comparison of medium range forecasts made with two parameterisation schemes. (1978)	Hollingsworth, A., K. Arpe, M. Tiedke, M. Capaldo, H. Sävijärvi, O. Åkesson, and J.A. Woods
14	On initial conditions for non-hydrostatic models. (1978)	Wiin-Nielsen, A.C.
15	Adiabatic formulation and organization of ECMWF's spectral model. (1979)	Baede, A.P.M., M. Jarraud, and U. Cubasch
16	Model studies of a developing boundary layer over the ocean. (1979)	Økland, H.
17	The response of a global barotropic model to forcing by large scale orography. (1980)	Quiby, J.
18	Confidence limits for verification and energetic studies. (1980)	Arpe, K.
19	A low order barotropic model on the sphere with orographic and newtonian forcing. (1980)	Källén, E.
20	A review of the normal mode initialization method. (1980)	Du Xing-yuan
21	The adjoint equation technique applied to meteorological problems. (1980)	Kontarev, G.
22	The use of empirical methods for mesoscale pressure forecasts. (1980)	Bergthorsson, P.
23	Comparison of medium range weather forecasts made with models using spectral or finite difference techniques in the horizontal. (1981)	Jarraud, M., C. Girard, and U. Cubasch
24	On the average errors of an ensemble of forecasts. (1981)	Derome, J.

25	On the atmospheric factors affecting the Levantine Sea. (1981)	Ozsoy, E.
26	Tropical influences on stationary wave motion in middle and high latitudes. (1981)	Simmons, A.J.
27	The energy budgets in North America, North Atlantic and Europe based on ECMWF analysis and forecasts. (1981)	Sävijärvi, H.
28	An energy and angular momentum conserving finite-difference scheme, hybrid coordinates and medium range weather forecasts. (1981)	Simmons, A.J., and R. Strüfing
29	Orographic influences on Mediterranean lee cyclogenesis and European blocking in a global numerical model. (1982)	Tibaldi, S. and A. Buzzi
30	Review and re-assessment of ECNET - A private network with open architecture. (1982)	Haag, A., Königshofer, F. and P. Quoilin
31	An investigation of the impact at middle and high latitudes of tropical forecast errors. (1982)	Haseler, J.
32	Short and medium range forecast differences between a spectral and grid point model. An extensive quasi-operational comparison. (1982)	Girard, C. and M. Jarraud
33	Numerical simulations of a case of blocking: The effects of orography and land-sea contrast. (1982)	Ji, L.R., and S. Tibaldi
34	The impact of cloud track wind data on global analyses and medium range forecasts. (1982)	Kållberg, P., S. Uppala, N. Gustafsson, and J. Pailleux
35	Energy budget calculations at ECMWF. Part 1: Analyses 1980-81. (1982)	Oriol, E.
36	Operational verification of ECMWF forecast fields and results for 1980-1981. (1983)	Nieminen, R.
37	High resolution experiments with the ECMWF model: a case study. (1983)	Dell'Osso, L.
38	The response of the ECMWF global model to the El-Niño anomaly in extended range prediction experiments. (1983)	Cubasch, U.
39	On the parameterisation of vertical diffusion in large-scale atmospheric models. (1983)	Manton, M.J.
40	Spectral characteristics of the ECMWF objective analysis system. (1983)	Daley, R.
41	Systematic errors in the baroclinic waves of the ECMWF. (1984)	Klinker, E., and M. Capaldo
42	On long stationary and transient atmospheric waves. (1984)	Wiin-Nielsen, A.C.
43	A new convective adjustment. (1984)	Betts, A.K., and M.J. Miller
44	Numerical experiments on the simulation of the 1979 Asian summer monsoon. (1984)	Mohanty, U.C., R.P. Pearce and M. Tiedtke
45	The effect of mechanical forcing on the formation of a mesoscale vortex. (1984)	Guo-xiong Wu and Shou-jun Chen
46	Cloud prediction in the ECMWF model. (1985)	Slingo, J., and B. Ritter
47	Impact of aircraft wind data on ECMWF analyses and forecasts during the FGGE period, 8-19 November. (1985)	Baede, A.P.M., P. Kållberg, and S. Uppala

48	A numerical case study of East Asian coastal cyclogenesis. (1985)	Chen, Shou-jun and L. Dell'Osso
49	A study of the predictability of the ECMWF operational forecast model in the tropics. (1985)	Kanamitsu, M.
50	On the development of orographic. (1985)	Radinović, D.
51	Climatology and systematic error of rainfall forecasts at ECMWF. (1985)	Molteni, F., and S. Tibaldi
52	Impact of modified physical processes on the tropical simulation in the ECMWF model. (1985)	Mohanty, U.C., J.M. Slingo and M. Tiedtke
53	The performance and systematic errors of the ECMWF tropical forecasts (1982-1984). (1985)	Heckley, W.A.
54	Finite element schemes for the vertical discretization of the ECMWF forecast model using linear elements. (1986)	Burridge, D.M., J. Steppeler, and R. Strüfing
55	Finite element schemes for the vertical discretization of the ECMWF forecast model using quadratic and cubic elements. (1986)	Steppeler, J.
56	Sensitivity of medium-range weather forecasts to the use of an envelope orography. (1986)	Jarraud, M., A.J. Simmons and M. Kanamitsu
57	Zonal diagnostics of the ECMWF operational analyses and forecasts. (1986)	Branković, Č.
58	An evaluation of the performance of the ECMWF operational forecasting system in analysing and forecasting tropical easterly disturbances. Part 1: Synoptic investigation. (1986)	Reed, R.J., A. Hollingsworth, W.A. Heckley and F. Delsol
59	Diabatic nonlinear normal mode initialisation for a spectral model with a hybrid vertical coordinate. (1987)	Wergen, W.
60	An evaluation of the performance of the ECMWF operational forecasting system in analysing and forecasting tropical easterly wave disturbances. Part 2: Spectral investigation. (1987)	Reed, R.J., E. Klinker and A. Hollingsworth
61	Empirical orthogonal function analysis in the zonal and eddy components of 500 mb height fields in the Northern extratropics. (1987)	Molteni, F.
62	Atmospheric effective angular momentum functions for 1986-1987. (1989)	Sakellarides, G.
63	A verification study of the global WAM model December 1987 - November 1988. (1989)	Zambresky, L.
64	Impact of a change of radiation transfer scheme in the ECMWF model. (1989)	Morcrette, J-J.
65	The ECMWF analysis-forecast system during AMEX. (1990)	Puri, K., P. Lönnberg and M. Miller
66	The calculation of geopotential and the pressure gradient in the ECMWF atmospheric model: Influence on the simulation of the polar atmosphere and on temperature analyses (1990)	Simmons, A.J. and Chen Jiabin
67	Assimilation of altimeter data in a global third generation wave model (1992)	Lionello, P., H. Günther and P. Janssen
68	Implementation of a third generation ocean wave model at the European Centre for Medium-Range Weather Forecasts (1992)	Günther, H., P. Lionello, P.A.E.M. Janssen et al.
69	A preliminary study of the impact of C-band scatterometer wind data on global scale numerical weather prediction (1992)	Hoffman, R.N.

70	Scientific assessment of the prospects for seasonal forecasting: a European perspective March 1993	Palmer, T.N. and D.L.T. Anderson
71	Results with a coupled wind-wave model February 1994	Janssen, P.A.E.M.
72	Implementation of the semi-Lagrangian method in a high resolution version of the ECMWF forecast model June 1994	Ritchie, H., C. Temperton, A. Simmons, M. Hortal, T. Davies, D. Dent and M. Hamrud